

Influences of the moving velocity and material property on frictionless contact problem of orthotropic materials indented by a moving punch

Y. T. ZHOU^{1,2)}, K. Y. LEE^{2,3)}, Y. H. JANG²⁾

¹⁾*School of Aerospace Engineering and Applied Mechanics
Tongji University, Shanghai 200092, P.R. China*

²⁾*School of Mechanical Engineering
Yonsei University, Seoul 120-749, Republic of Korea*

³⁾*State Key Laboratory of Structural Analysis for Industrial Equipment
Department of Engineering Mechanics
Dalian University of Technology, Dalian 116024, P.R. China
e-mails: kylee@dlut.edu.cn and KYL2813@yonsei.ac.kr*

IN ANALYZING THE CONTACT BEHAVIOR of a material indented by a moving punch, of much importance are the contributions of the moving velocity and material property. The present paper develops a smoothly moving contact model for orthotropic materials indented by a rigid punch. Based on fundamental solutions of each eigenvalue case, the mixed boundary-value problem is reduced to a Cauchy type singular integral equation by applying the Galilean transformation and Fourier transform. Particularly, the exact solution of the obtained singular integral equation is presented, and closed-form expressions of the physical quantities are given for a flat punch and a cylindrical punch. Figures are plotted to show the influences of the moving velocity, material properties and other loadings on the contact behaviors and to reveal the surface damage mechanism, which may provide useful guidelines for material's designing and optimization.

Key words: orthotropic materials, moving velocity, material property, real fundamental solutions, exact solutions.

Copyright © 2013 by IPPT PAN

1. Introduction

THE HISTORY OF CONTACT ANALYSIS of deformable components began in 1882, when HERTZ [1] analytically addressed the load distributions over a contact area and obtained the stresses in the body by using the Newtonian potential function. The contact problems are often reduced to mixed boundary-value problems with unknown or moving boundaries. Thus, analytical solutions are of great importance due to that challenging nature. For two-dimensional (2D) and axisymmetric contact problems in linear elastic bodies, there were some analytical solutions [2–4].

However, contact problems are often difficult to be solved accurately. A significant amount of research work has been conducted by applying either experimental techniques or numerical methods. For example, photoelastic experimental hybrid methods were used to evaluate contact stress and internal stress of an O-ring under a uniform squeeze rate [5]. Numerical techniques based on computer technology have drawn researchers' attention in investigating contact problems. For example, CONRY and SEIREG [6], among early researchers who used numerical analysis [7, 8] in contact problems, employed the simplex method to determine the displacement and pressure distribution in the contact zone between two contacting spheres. With the computer capacity greatly increasing, finite element methods [9, 10] were most widely employed in solving contact problems. Though finite element methods may solve contact problems with more complicated geometry and material properties, they have a main drawback of depending upon the number of elements and element types used to analyze the stated problem. To improve the computational efficiency needed in finite element methods, a novel method named pseudo-interference stiffness estimation [11], for evaluating the contact compliance and the contact load in the contacting elastic solids, was proposed and its results were comparable to finite element contact analysis.

The above-mentioned examples concerned contact problem involving isotropic or transversely isotropic materials. Contact problems of orthotropic materials [12] are of interest in a number of applications, including those related to foreign body impact in composite materials. PAGANO [13] presented the solution of layered orthotropic materials with simply supported edges, which was given in terms of Fourier's series expansions of transverse pressure loading. Since it was difficult to get exact solutions, numerical methods were applied. Using a nine-node isoparametric plate finite element in conjunction with an empirical contact law, TAN and SUN [14] investigated the low-velocity impact response of orthotropic graphite/epoxy laminates. The contact behavior between composite laminates and rigid spheres was discussed by WU and YEN [15] employing a method derived from the three-dimensional anisotropic elasticity theory. To expand and clarify the theoretical development and numerical solution of SVEKLO's analysis [16–18] for indentation of an orthotropic half-space, SHI *et al.* [19] conducted an analysis of indentation by a rigid ellipsoidal indenter against an orthotropic half-space with the surface of the half-space parallel to two of the axes of material symmetry. Combining Willis' solution of axisymmetric contact problem [20] with the solution of PAGANO [13], SWANSON [21] proposed a procedure to determine the contact area and pressure distribution for orthotropic materials. In the references mentioned above, the single punch was stationary and most results were based on numerical methods. DE and PATRA [22] treated the frictionless dynamic punch problems in an orthotropic half-space, where explicit

expressions of stress components under the triangular punch were presented in terms of elementary functions. For frictionally dynamic contact, IAMANIDZE and LOSABERIDZE [23] examined the dynamic effect caused by moving punches on an isotropic elastic half-plane with the account of friction force with results given in integral form. To the authors' knowledge, exact solutions of the dynamic contact problem of orthotropic materials subjected to a flat or cylindrical punch in terms of elementary functions have not been reported due to the mathematical complexity involved.

The present paper considers an exact contact analysis for orthotropic materials under a rigid punch. The rigid punch, which occupies a flat or cylindrical profile, smoothly moves at a constant velocity on the surface of orthotropic materials. It is convenient to introduce the Galilean transformation to address the time-related problem. Then applying the Galilean transformation and Fourier transform, the exact solutions of the singular integral equation are obtained. Based on these exact solutions, closed-form expressions of physical quantities in terms of the elementary functions are presented for either a flat punch or a cylindrical punch. Stress intensity factor at the edges of the flat punch is defined. Formula to determine the unknown contact beneath the cylindrical punch is given. Numerical results are given to demonstrate the influences of the moving velocity, material properties and other loadings on contact behavior.

2. The general model for the moving contact problem

Figure 1 shows a schematic representation of the moving contact model under consideration: orthotropic half-plane materials indented by a rigid punch moving smoothly at a constant speed V in the positive direction of the x axis. The rigid stamp possesses either a flat profile or a cylindrical profile.

The standard generalized Hooke's law for orthotropic materials in a state of plane stress is as follows:

$$(2.1) \quad \begin{bmatrix} \sigma_{xx} \\ \sigma_{yy} \\ \sigma_{xy} \end{bmatrix} = \begin{bmatrix} D_{11} & D_{12} & D_{13} \\ D_{21} & D_{22} & D_{23} \\ D_{31} & D_{32} & D_{33} \end{bmatrix} \begin{bmatrix} \varepsilon_{xx} \\ \varepsilon_{yy} \\ 2\varepsilon_{xy} \end{bmatrix},$$

where σ_{xx} , σ_{yy} and σ_{xy} are components of stress, and strain $\varepsilon_{\alpha\beta}$ ($\alpha, \beta = x, y$) is given as

$$(2.2) \quad \varepsilon_{\alpha\beta} = \frac{1}{2}(u_{\alpha,\beta} + u_{\beta,\alpha}),$$

where a subscript after a comma designates a partial derivative, $u_x = u$ and $u_y = v$ are elastic displacements.

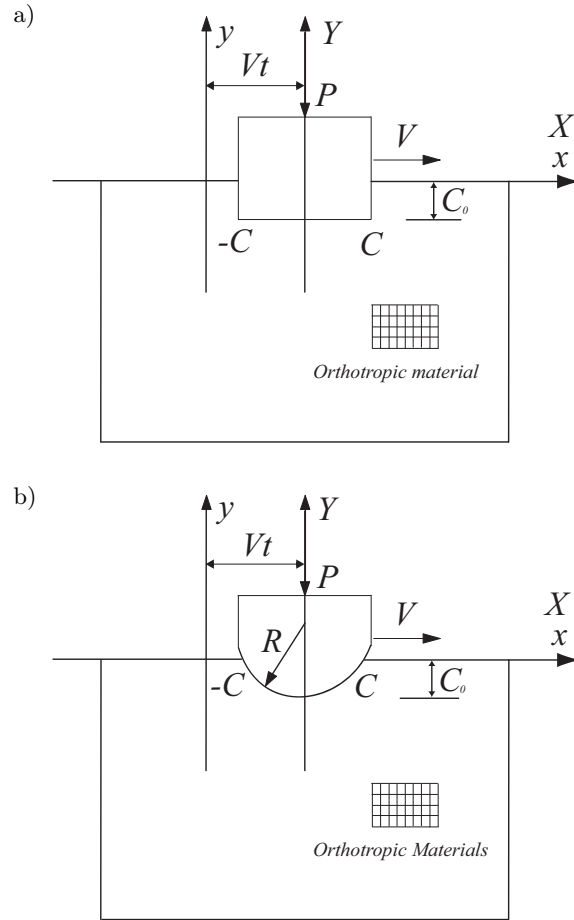


FIG. 1. Moving contact model for orthotropic materials indented by a moving punch with
a) flat profile, b) cylindrical profile.

In Eq. (2.1), the elements D_{ij} of the symmetric coefficient matrix depend on five material constants and are given as

$$(2.3) \quad \begin{aligned} D_{11} &= \frac{E_{xx}}{1 - \nu_{xy}\nu_{yx}}, & D_{12} &= \frac{E_{xx}\nu_{yx}}{1 - \nu_{xy}\nu_{yx}} = \frac{E_{yy}\nu_{xy}}{1 - \nu_{xy}\nu_{yx}}, \\ D_{22} &= \frac{E_{yy}}{1 - \nu_{xy}\nu_{yx}}, & D_{13} &= D_{23} = 0, & D_{33} &= G_{xy}, \end{aligned}$$

where E_{xx} and E_{yy} stand for Young's moduli, G_{xy} is the shear modulus, and ν_{xy} and ν_{yx} represent Poisson's ratios.

The equations of motion are given as follows:

$$(2.4) \quad \sigma_{xx,x} + \sigma_{xy,y} = \rho\ddot{u},$$

$$(2.5) \quad \sigma_{xy,x} + \sigma_{yy,y} = \rho\ddot{v}.$$

The equations of motion may be expressed exclusively in terms of displacement derivatives by substituting strain components in terms of displacement derivatives into Eq. (2.1) and the latter into Eqs. (2.4) and (2.5)

$$(2.6) \quad D_{11}u_{,xx} + D_{33}u_{,yy} + D_{13}v_{,xx} + D_{23}v_{,yy} + 2D_{13}u_{,xy} + (D_{12} + D_{33})v_{,xy} = \rho\ddot{u},$$

$$(2.7) \quad D_{13}u_{,xx} + D_{23}u_{,yy} + D_{33}v_{,xx} + D_{22}v_{,yy} + (D_{12} + D_{33})u_{,xy} + 2D_{23}v_{,xy} = \rho\ddot{v}.$$

In Eqs. (2.4)–(2.7), \ddot{u} and \ddot{v} denote second-order derivations with respect to time t , and ρ is the mass density.

Galilean transformation is introduced

$$(2.8) \quad X = x - Vt, \quad y = Y,$$

with (X, Y) being a translating coordinate system, which is attached to the punch.

Substitution of Eq. (2.8) into Eqs. (2.6) and (2.7) yields the steady-state governing equations in the coordinate system (X, Y)

$$(2.9) \quad (D_{11} - D_{33}c^2)u_{,XX} + D_{33}u_{,YY} + D_{13}v_{,XX} + D_{23}v_{,YY} \\ + 2D_{13}u_{,XY} + (D_{12} + D_{33})v_{,XY} = 0,$$

$$(2.10) \quad D_{13}u_{,XX} + D_{23}u_{,YY} + D_{33}(1 - c^2)v_{,XX} + D_{22}v_{,YY} \\ + (D_{12} + D_{33})u_{,XY} + 2D_{23}v_{,XY} = 0,$$

where $c = V/c_v$ is the relative moving velocity of the punch, and $c_v = \sqrt{D_{33}/\rho}$ is the lowest bulk wave velocity.

3. Fundamental solutions

Applying Fourier's sine and cosine transforms with the transform variable ω

$$(3.1) \quad [U(\omega, Y), V(\omega, Y)] = \int_0^\infty [u(X, Y) \sin(\omega X), v(X, Y) \cos(\omega X)] dX$$

to Eqs. (2.9) and (2.10), and using the following expressions

$$(3.2) \quad [U(\omega, Y), V(\omega, Y)] = [U_0, V_0]e^{\tau\omega Y},$$

one can get the following characteristic equation in terms of τ :

$$(3.3) \quad \tau^4 + A\tau^2 + B = 0,$$

where

$$(3.4) \quad A = \frac{(D_{12} + D_{33})^2 - (D_{33})^2(1 - c^2) - D_{22}(D_{11} - D_{33}c^2)}{D_{22}D_{33}},$$

$$B = \frac{(D_{11} - D_{33}c^2)D_{33}(1 - c^2)}{D_{22}D_{33}}.$$

The eigenvalue distribution is dependent on the materials' coefficients and plays a key role in the development of the solution. In the present article only unequal eigenvalues are considered to make the analytical solutions in terms of elementary function available. From the point of view of mathematics, the roots of Eq. (3.3) are of the following cases: (i) two pairs of opposite real roots, (ii) two pairs of complex conjugate roots (no purely imaginary roots), (iii) one pair of opposite real roots and one pair of purely imaginary roots, and (iv) two pairs of purely imaginary roots. From the point of view of physics, only case (i) and case (ii) with positive real part hold since the solution of a semi-infinite orthotropic plane should satisfy the regularity conditions at infinity, i.e., Eqs. (4.1) and (4.2) given latter. For case (i) and case (ii), the transformed quantities $[U(\omega, Y), V(\omega, Y)]$ will be expressed by real fundamental solutions for each case.

Case (i): two pairs of opposite real roots

$$(3.5) \quad \tau_1 = -\tau_3 = o_1, \quad \tau_2 = -\tau_4 = o_2,$$

where $o_n > 0 (n = 1, 2)$.

In this case, the transformed quantities $[U(\omega, Y), V(\omega, Y)]$ can be obtained as

$$(3.6) \quad U(\omega, Y) = \sum_{n=1}^2 A_n e^{o_n \omega Y},$$

$$(3.7) \quad V(\omega, Y) = \sum_{n=1}^2 l(o_n) A_n e^{o_n \omega Y},$$

where function $l(\tau)$ is given as

$$(3.8) \quad l(\tau) = \frac{D_{33}\tau^2 - D_{11} + D_{33}c^2}{(D_{12} + D_{33})\tau}.$$

Case (ii): two pairs of complex conjugate roots

$$(3.9) \quad \tau_1 = -\tau_3 = \alpha + i\beta, \quad \tau_2 = -\tau_4 = \alpha - i\beta,$$

where $i^2 = -1$, $\alpha > 0$ and β is a real number.

In this case, the transformed quantities $[U(\omega, Y), V(\omega, Y)]$ can be obtained

$$(3.10) \quad U(\omega, Y) = \sum_{n=1}^2 M_{1n}(\omega, Y) A_n e^{\alpha\omega Y},$$

$$(3.11) \quad V(\omega, Y) = \sum_{n=1}^2 M_{2n}(\omega, Y) A_n e^{\alpha\omega Y},$$

where $M_{mn}(\omega, Y)$ ($m, n = 1, 2$) are given as

$$(3.12) \quad \begin{aligned} M_{11}(\omega, Y) &= \cos(\beta\omega Y), & M_{12}(\omega, Y) &= \sin(\beta\omega Y), \\ M_{21}(\omega, Y) &= \operatorname{Re}[l(\tau_1)] \cos(\beta\omega Y) - \operatorname{Im}[l(\tau_1)] \sin(\beta\omega Y), \\ M_{22}(\omega, Y) &= \operatorname{Im}[l(\tau_1)] \cos(\beta\omega Y) + \operatorname{Re}[l(\tau_1)] \sin(\beta\omega Y), \end{aligned}$$

where $\operatorname{Re}[\cdot]$ and $\operatorname{Im}[\cdot]$ represent real part and imaginary part, respectively.

Considering Eqs. (3.6), (3.7), (3.10), (3.11), (2.8) and (2.1) produces the following expressions of stresses:

$$(3.13) \quad \begin{aligned} [\sigma_{XX}, \sigma_{YY}, \tau_{XY}] &= \frac{2}{\pi} \int_0^\infty \sum_{n=1}^2 \omega A_n \\ &\times [\Theta_{1n}(\omega, Y) \cos(\omega X), \Theta_{2n}(\omega, Y) \cos(\omega X), \Theta_{3n}(\omega, Y) \sin(\omega X)] d\omega, \end{aligned}$$

where functions $\Theta_{mn}(\omega, Y)$ ($m = 1, 2, 3, n = 1, 2$) are given in Appendix A.

In Eqs. (3.6), (3.7), (3.10), (3.11) and (3.13), A_n ($n = 1, 2$) are unknown functions to be determined from boundary conditions.

4. Boundary conditions and integral equation

Boundary conditions can be given in the coordinate system (X, Y) . Regularity conditions should also be satisfied

$$(4.1) \quad u(X, Y) \rightarrow 0, \quad \sqrt{X^2 + Y^2} \rightarrow \infty,$$

$$(4.2) \quad v(X, Y) \rightarrow 0, \quad \sqrt{X^2 + Y^2} \rightarrow \infty.$$

The penetration depth of the rigid punch is known a priori. For a flat punch, the penetration depth is

$$(4.3) \quad v(X, 0) = -C_0, \quad |X| < C,$$

and for a cylindrical, it is

$$(4.4) \quad v(X, 0) = -C_0 + \frac{X^2}{2R}, \quad |X| < C,$$

where C_0 is a constant, C is the half-length of the contact region, and R is the radius of the cylindrical punch.

Since the punch moves smoothly, the shear stress is free on the surface, i.e.,

$$(4.5) \quad \sigma_{XY}(X, 0) = 0, \quad |X| < +\infty.$$

The normal stress is unknown inside the contact region and is free outside the contact region

$$(4.6) \quad \sigma_{YY}(X, 0) = -p(X), \quad |X| < C,$$

$$(4.7) \quad \sigma_{YY}(X, 0) = 0, \quad |X| > C,$$

where $p(X)$ is unknown surface contact stress inside the contact region.

Equilibrium condition should be satisfied

$$(4.8) \quad \int_{-a}^a p(X) dX = P,$$

where P stands for the indentation force applied on the punch along the Y -axis.

With consideration of boundary conditions Eqs. (4.5)–(4.7), the following expressions are obtained for unknown functions Λ_n ($n = 1, 2$):

$$(4.9) \quad \Lambda_n = \frac{G_0 Q_n}{\omega},$$

where Q_n ($n = 1, 2$) are given as

$$(4.10) \quad Q_1 = -\Theta_{32}(\omega, 0) \left/ \begin{vmatrix} \Theta_{21}(\omega, 0) & \Theta_{22}(\omega, 0) \\ \Theta_{31}(\omega, 0) & \Theta_{32}(\omega, 0) \end{vmatrix} \right.,$$

$$Q_2 = \Theta_{31}(\omega, 0) \left/ \begin{vmatrix} \Theta_{21}(\omega, 0) & \Theta_{22}(\omega, 0) \\ \Theta_{31}(\omega, 0) & \Theta_{32}(\omega, 0) \end{vmatrix} \right.$$

and G_0 is

$$(4.11) \quad G_0 = \int_0^C p(\eta) \cos(\omega\eta) d\eta.$$

Considering Eqs. (4.9), (3.7), (3.11) and (3.1) yields

$$(4.12) \quad \frac{\partial v(X, 0)}{\partial X} = \frac{2}{\pi} \int_0^a \int_0^\infty L_a p(\eta) \cos(\omega\eta) \sin(\omega X) d\omega d\eta,$$

with the kernel L_a given as

$$(4.13) \quad L_a = - \sum_{n=1}^2 W_n Q_n,$$

where

$$(4.14) \quad W_n = \begin{cases} l(o_n), & \text{Case (i),} \\ M_{2n}(\omega, 0), & \text{Case (ii).} \end{cases}$$

After separating the singularity, Eq. (4.12) can be rewritten into the following singular integral equation:

$$(4.15) \quad \int_{-a}^a \frac{L_a}{\eta - X} p(\eta) d\eta = - \frac{\partial v(X, 0)}{\partial X} \pi.$$

When solving Eq. (4.15), the equilibrium equation (4.8) should be considered. In what follows, exact solution of integral equations (4.15) and (4.8) will be given and explicit expressions of various stresses will be presented.

5. Exact solution

5.1. Exact solutions for a flat punch

In this case, considering Eq. (4.3), one can obtain the exact solution of integral equations (4.15) and (4.8) as follows:

$$(5.1) \quad p(X) = \frac{P}{\pi\sqrt{C^2 - X^2}}, \quad |X| < C.$$

With substitution of Eq. (5.1) into Eq. (4.11), one can rewrite unknown functions A_n ($n = 1, 2$) in case of a flat punch as

$$(5.2) \quad A_n = \frac{PQ_n}{2\omega} J_0(\omega C),$$

where $J_0(\cdot)$ stands for the zero-order Bessel function of the first kind.

Substituting Eq. (5.2) into Eq. (3.13) leads to the closed-form expressions of various stresses

$$(5.3) \quad [\sigma_{XX}, \sigma_{YY}, \tau_{XY}] = \frac{P}{\pi} \sum_{n=1}^2 Q_n [\mathbf{T}_{1n}(X, Y), \mathbf{T}_{2n}(X, Y), \mathbf{T}_{3n}(X, Y)],$$

where known functions $\mathbf{T}_{mn}(X, Y)$ ($m = 1, 2, 3$, $n = 1, 2$) are given in Appendix A.

For the flat punch, the following stress intensity factor at the punch edge may be defined:

$$(5.4) \quad F_s = \lim_{X \rightarrow C^-} \sqrt{2\pi(C - X)} \sigma_{YY}(X, 0),$$

which can be rewritten as

$$(5.5) \quad F_s = -P/\sqrt{C\pi}.$$

5.2. Exact solutions for a cylindrical punch

In this case, considering Eq. (27), one can obtain the exact solution of integral equation (38) as follows:

$$(5.6) \quad p(X) = \frac{\sqrt{C^2 - X^2}}{L_a R}, \quad |X| < C.$$

Substituting Eq. (5.6) into Eq. (4.11), one can rewrite unknown functions A_n ($n = 1, 2$) in case of a cylindrical punch as

$$(5.7) \quad A_n = \frac{C\pi Q_n}{2\omega^2 L_a R} J_1(\omega C),$$

where $J_1(\cdot)$ represents the first-order Bessel function of the first kind.

Substituting Eq. (5.7) into Eq. (3.13) leads to the closed-form expressions of various stresses

$$(5.8) \quad [\sigma_{XX}, \sigma_{YY}, \tau_{XY}] = \frac{C}{L_a R} \sum_{n=1}^2 Q_n [\mathbf{I}_{1n}(X, Y), \mathbf{I}_{2n}(X, Y), \mathbf{I}_{3n}(X, Y)],$$

where known functions $\mathbf{I}_{mn}(X, Y)$ ($m = 1, 2, 3$, $n = 1, 2$) are given in Appendix A.

It should be noted that different from the flat punch with known contact region, the contact region of the cylindrical punch is unknown a priori, which can be determined by the following relationship between the half-width C of the contact region and the indentation force P :

$$(5.9) \quad C = \sqrt{\frac{2PL_a R}{\pi}}.$$

6. Numerical results

Numerical calculations are carried out for carbon-fiber-reinforced plastic. The material constants for carbon-fiber-reinforced plastic are $E_{xx} = E_{xx0}$ ($E_{xx0} = 145$ GPa), $E_{yy} = E_{yy0}$ ($E_{yy0} = 9.6$ GPa), $G_{xy} = 4.8$ GPa, $\nu_{xy} = 0.23$ and $\nu_{yx} = E_{yy}\nu_{xy}/E_{xx}$ [24].

6.1. Contact behavior under a moving flat punch

Figure 2 depicts the distribution of the normalized surface normal stress $\sigma_{YY}(X/C, 0)/\sigma_0$ ($\sigma_0 = P/(a\pi)$) under the moving flat punch. Figure 2 can be drawn either from Eq. (5.1) in view of Eq. (4.6) or from the second expression of Eq. (5.3), which justifies the correctness of the derivation for the case of the flat punch.

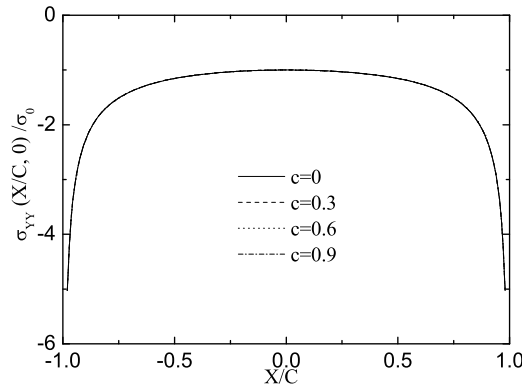


FIG. 2. The distribution of the normalized surface normal stress $\sigma_{YY}(X/C, 0)/\sigma_0$ under a moving flat punch.

It can be observed that a serious normal stress concentration occurs in the vicinity of the flat punch edges, at which cracks may originate and propagate to cause surface damage. The surface normal stress is independent of velocity c , which can be verified from Eq. (5.1) in view of Eq. (4.6). In fact, the surface normal stress is also independent of the Young's modulus ratios E_{xx}/E_{xx0} and E_{yy}/E_{yy0} , which means that the material properties have no effects on the surface normal stress under a flat punch. The influence of velocity c and Young's modulus ratios E_{xx}/E_{xx0} and E_{yy}/E_{yy0} on normalized normal stress $\sigma_{YY}(X/C, Y/C)/\sigma_0$ inside orthotropic materials under the moving flat punch is depicted in Figs. 3–5. Different from the surface normal stress, velocity c and Young's modulus ratios E_{xx}/E_{yy0} greatly affect the distribution of the normal stress inside orthotropic materials. There are the following common features shown in these figures: (i) the normal stress is continuous everywhere inside orthotropic materials and tends to

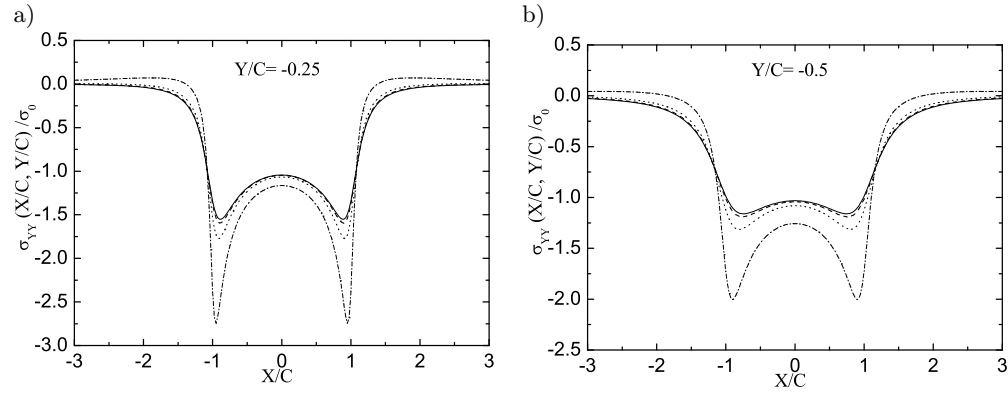


FIG. 3. The influence of velocity c on the normalized normal stress $\sigma_{YY}(X/C, Y/C)/\sigma_0$ under a moving flat punch; — $c = 0$, --- $c = 0.3$, \cdots $c = 0.6$, - · - · $c = 0.9$.

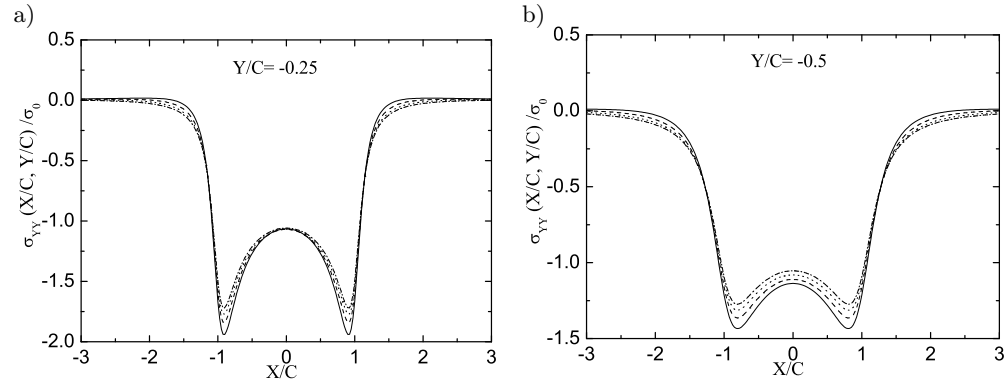


FIG. 4. The influence of ratio E_{xx}/E_{xx0} on the normalized normal stress $\sigma_{YY}(X/C, Y/C)/\sigma_0$ under a moving flat punch with $c = 0.6$; — $E_{xx}/E_{xx0} = 0.25$, --- $E_{xx}/E_{xx0} = 0.5$, \cdots $E_{xx}/E_{xx0} = 1$, - · - · $E_{xx}/E_{xx0} = 1$, - · - · - $E_{xx}/E_{xx0} = 2$.

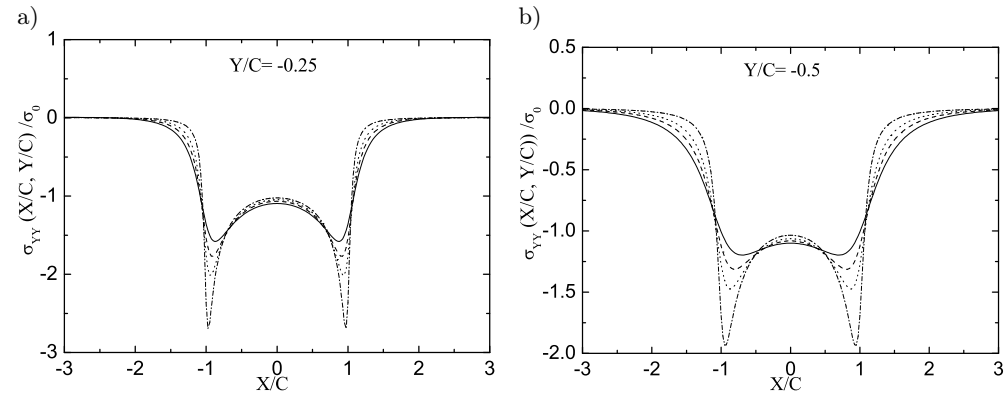


FIG. 5. The influence of ratio E_{yy}/E_{yy0} on the normalized normal stress $\sigma_{YY}(X/C, Y/C)/\sigma_0$ under a moving flat punch with $c = 0.6$; — $E_{yy}/E_{yy0} = 0.5$, --- $E_{yy}/E_{yy0} = 1$, \cdots $E_{yy}/E_{yy0} = 2$, - · - · $E_{yy}/E_{yy0} = 2$, - · - · - $E_{yy}/E_{yy0} = 8$.

vanish rapidly as the magnitude of X/a increases, which meets the requirement of the regularity conditions given in Eqs. (4.1) and (4.2), (ii) the peak magnitude of the normal stress appears at the locations near the punch edges, and (iii) the bigger the value of velocity c and Young's modulus ratios E_{xx}/E_{xx0} and E_{yy}/E_{yy0} , the nearer the locations from the flat punch edges. In addition, Fig. 3 shows that the peak magnitude of the normal stress increases with velocity c . The peak magnitude of the normal stress decreases as Young's modulus ratio E_{xx}/E_{xx0} becomes larger as indicated in Fig. 4. Figure 5 demonstrates that increasing Young's modulus ratio E_{yy}/E_{yy0} results in a bigger peak magnitude of the normal stress.

Figure 6 shows the distribution of the normalized surface in-plane stress $\sigma_{XX}(X/C, 0)/\sigma_0$ under the moving flat punch for various velocities c and the Young's modulus ratios E_{xx}/E_{xx0} and E_{yy}/E_{yy0} . It is found that the normalized surface in-plane stress $\sigma_{XX}(X/C, 0)/\sigma_0$ is discontinuous around the edges of the flat punch, and there is a serious in-plane stress concentration around the edges

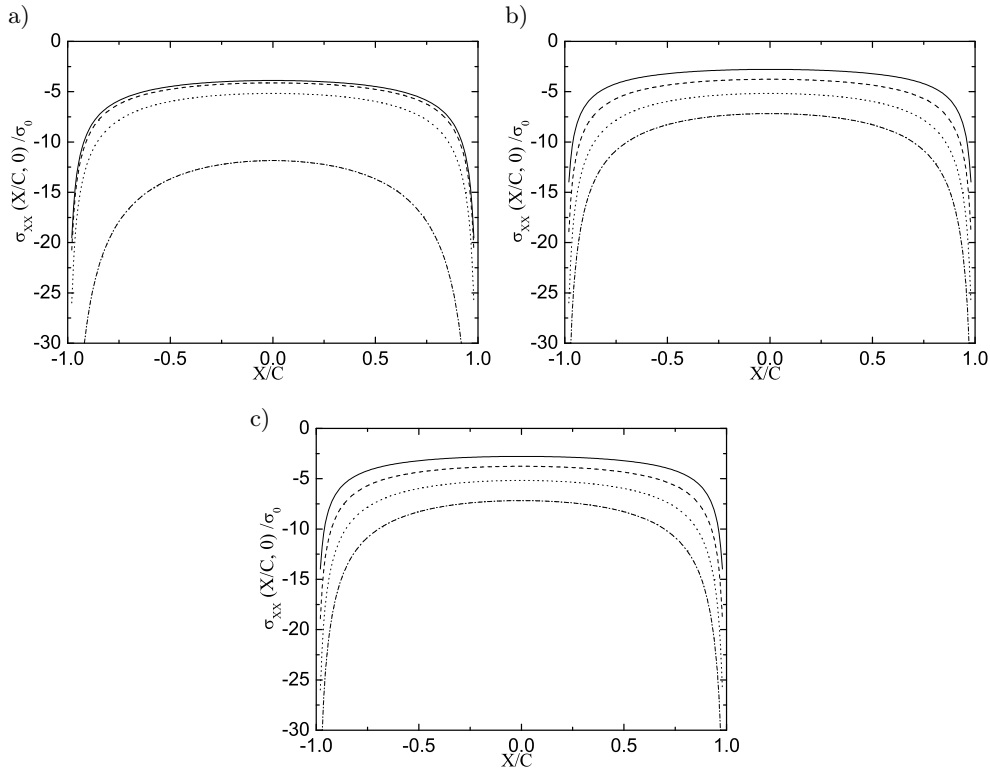


FIG. 6. The influence of a) velocity c , — $c = 0$, --- $c = 0.3$, \cdots $c = 0.6$, - · - · - $c = 0.9$ b) ratio E_{xx}/E_{xx0} with $c = 0.6$, — $E_{xx}/E_{xx0} = 0.25$, --- $E_{xx}/E_{xx0} = 0.5$, \cdots $E_{xx}/E_{xx0} = 1$, - · - · - $E_{xx}/E_{xx0} = 2$, c) ratio E_{yy}/E_{yy0} with $c = 0.6$, — $E_{yy}/E_{yy0} = 0.5$, --- $E_{yy}/E_{yy0} = 1$, \cdots $E_{yy}/E_{yy0} = 2$, - · - · - $E_{yy}/E_{yy0} = 8$, on the normalized surface in-plane stress $\sigma_{XX}(X/C, 0)/\sigma_0$ under a moving flat punch.

of the punch, which may account for surface damage under the punch. To avoid the surface damage, each of the following ways can be employed: (i) reducing the moving velocity of the flat punch, (ii) decreasing the Young's modulus ratio E_{xx}/E_{xx0} , or (iii) increasing the Young's modulus ratio E_{yy}/E_{yy0} .

6.2. Contact behavior under a moving cylindrical punch

The contact region between a cylindrical punch and an orthotropic solid is unknown a priori and can be determined by Eq. (5.9). Figure 7 examines the influence of velocity c , indentation force P , and Young's modulus ratios E_{xx}/E_{xx0} and E_{yy}/E_{yy0} on the contact region. It can be seen that increasing the radius R results in a wider contact region. Figure 7 also illustrates that the contact region can also become wider through each of the following ways: a) enhancing the moving velocity, b) increasing the indentation force P , c) decreasing Young's modulus ratio E_{xx}/E_{xx0} , and d) decreasing Young's modulus ratio E_{yy}/E_{yy0} . These conclusions are further confirmed later.

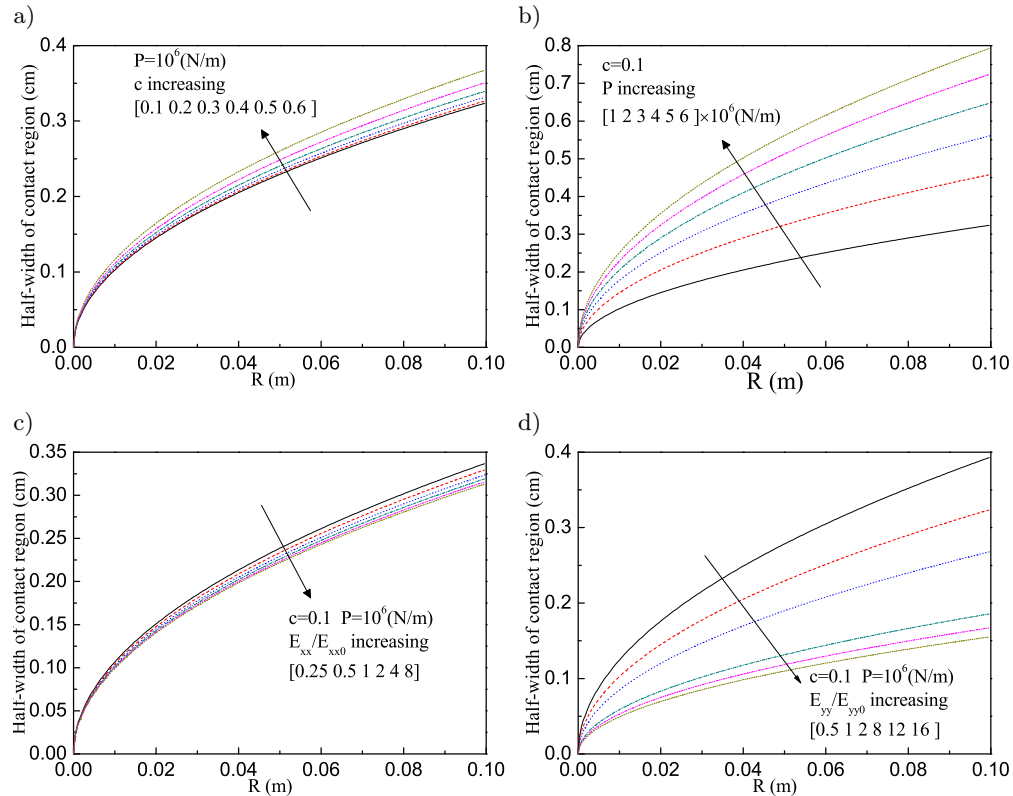


FIG. 7. The influence of a) velocity c , b) indentation force P , c) ratio E_{xx}/E_{xx0} , and d) ratio E_{yy}/E_{yy0} on the contact length under a moving cylindrical punch.

The influence of velocity c , indentation force P , radius R , ratio E_{xx}/E_{xx0} , and ratio E_{yy}/E_{yy0} on the surface normal stress $\sigma_{YY}(X, 0)$ under the moving cylindrical punch is shown in Fig. 8. It is observed that the surface normal stress $\sigma_{YY}(X, 0)$ is zero at the edges of the cylindrical punch. As discussed in

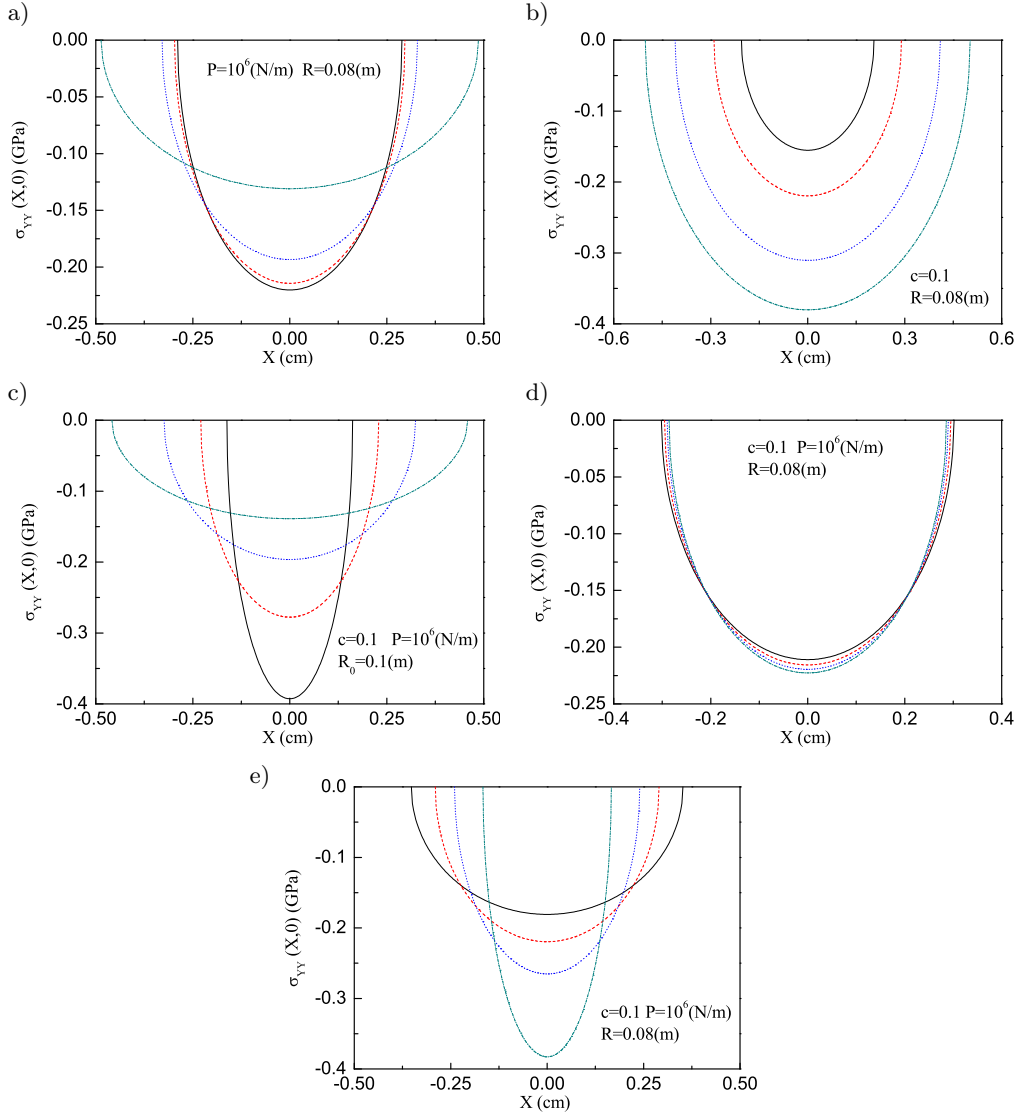


FIG. 8. The influence of a) velocity c , --- $c = 0.3$, \cdots $c = 0.6$, - - - - $c = 0.9$, b) indentation force P , — $P = 0.5 \times 10^6$ N/m, - - - $P = 1 \times 10^6$ N/m, \cdots $P = 3 \times 10^6$ N/m, - - - - $P = 3 \times 10^6$ N/m, c) radius R , — $R = 0.25 \times R_0$, - - - $R = 0.5 \times R_0$, \cdots $R = 1 \times R_0$, - - - - $R = 2 \times R_0$, d) ratio E_{xx}/E_{xx0} , — $E_{xx}/E_{xx0} = 0.25$, - - - $E_{xx}/E_{xx0} = 0.5$, \cdots $E_{xx}/E_{xx0} = 1$, - - - - $E_{xx}/E_{xx0} = 2$, e) ratio E_{yy}/E_{yy0} , — $E_{yy}/E_{yy0} = 0.5$, - - - $E_{yy}/E_{yy0} = 1$, \cdots $E_{yy}/E_{yy0} = 2$, - - - - $E_{yy}/E_{yy0} = 8$, on the surface normal stress $\sigma_{YY}(X, 0)$ under a moving cylindrical punch.

Subsection 6.1, the surface contact stress is singular at the edges of the flat punch. Thus, the punch profile plays a key role in the contact problem.

Figure 8 reconfirms the conclusions made in Fig. 7 about the influences of various parameters on the contact region. The peak magnitude of the surface

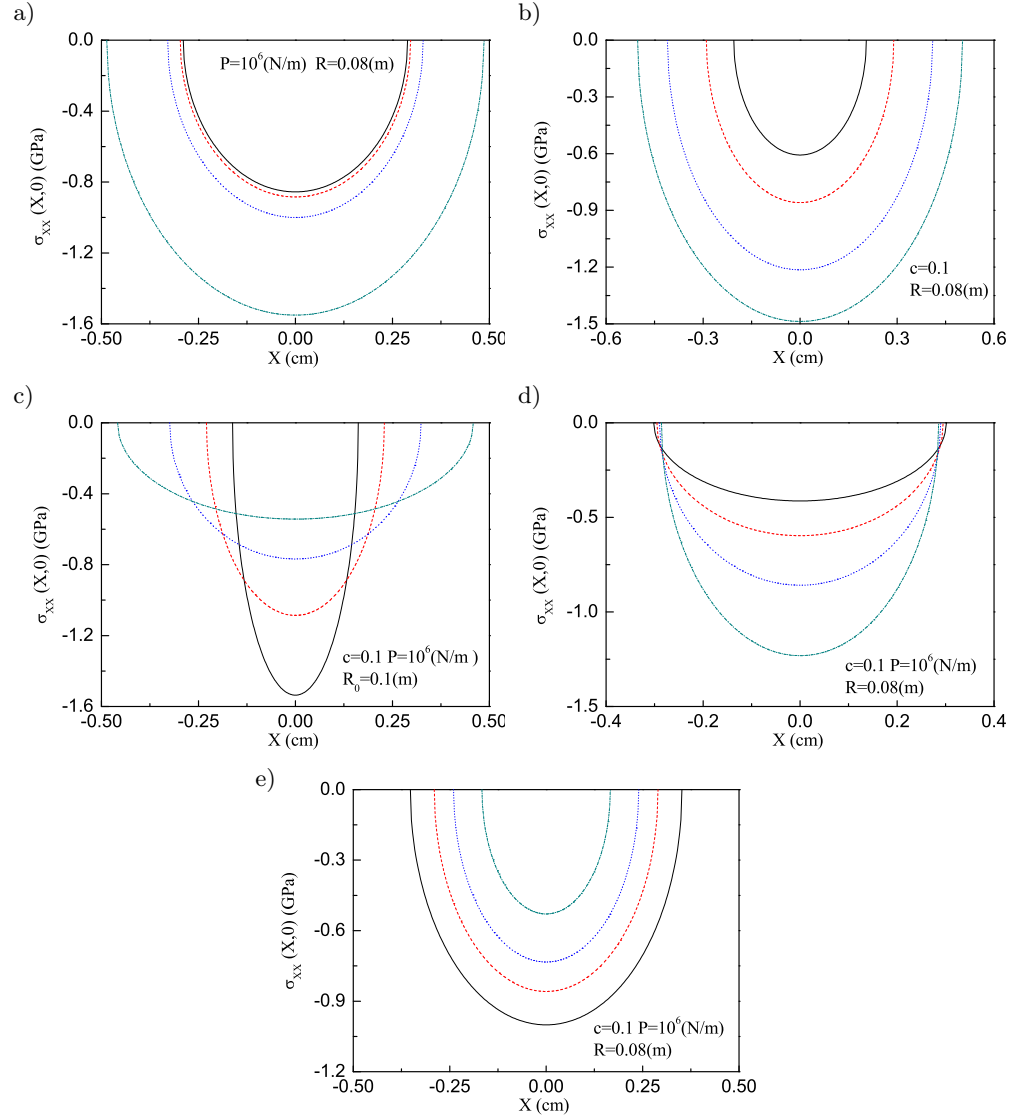


FIG. 9. The influence of a) velocity c , --- $c = 0.3$, \cdots $c = 0.6$, - - - - $c = 0.9$, b) indentation force P , — $P = 0.5 \times 10^6$ N/m, --- $P = 1 \times 10^6$ N/m, \cdots $P = 3 \times 10^6$ N/m, - - - - $P = 3 \times 10^6$ N/m, c) radius R , — $R = 0.25 \times R_0$, --- $R = 0.5 \times R_0$, \cdots $R = 1 \times R_0$, - - - - $R = 2 \times R_0$, d) ratio E_{xx}/E_{xx0} , — $E_{xx}/E_{xx0} = 0.25$, --- $E_{xx}/E_{xx0} = 0.5$, \cdots $E_{xx}/E_{xx0} = 1$, - - - - $E_{xx}/E_{xx0} = 2$, e) ratio E_{yy}/E_{yy0} , — $E_{yy}/E_{yy0} = 0.5$, --- $E_{yy}/E_{yy0} = 1$, \cdots $E_{yy}/E_{yy0} = 2$, - - - - $E_{yy}/E_{yy0} = 8$, on the surface normal stress $\sigma_{XX}(X, 0)$ under a moving cylindrical punch.

normal stress $\sigma_{YY}(X, 0)$ always appears at the punch center, which can be relieved by using each of the following ways: a) enhancing the moving velocity, b) decreasing the indentation force P , c) increasing the radius R , d) decreasing

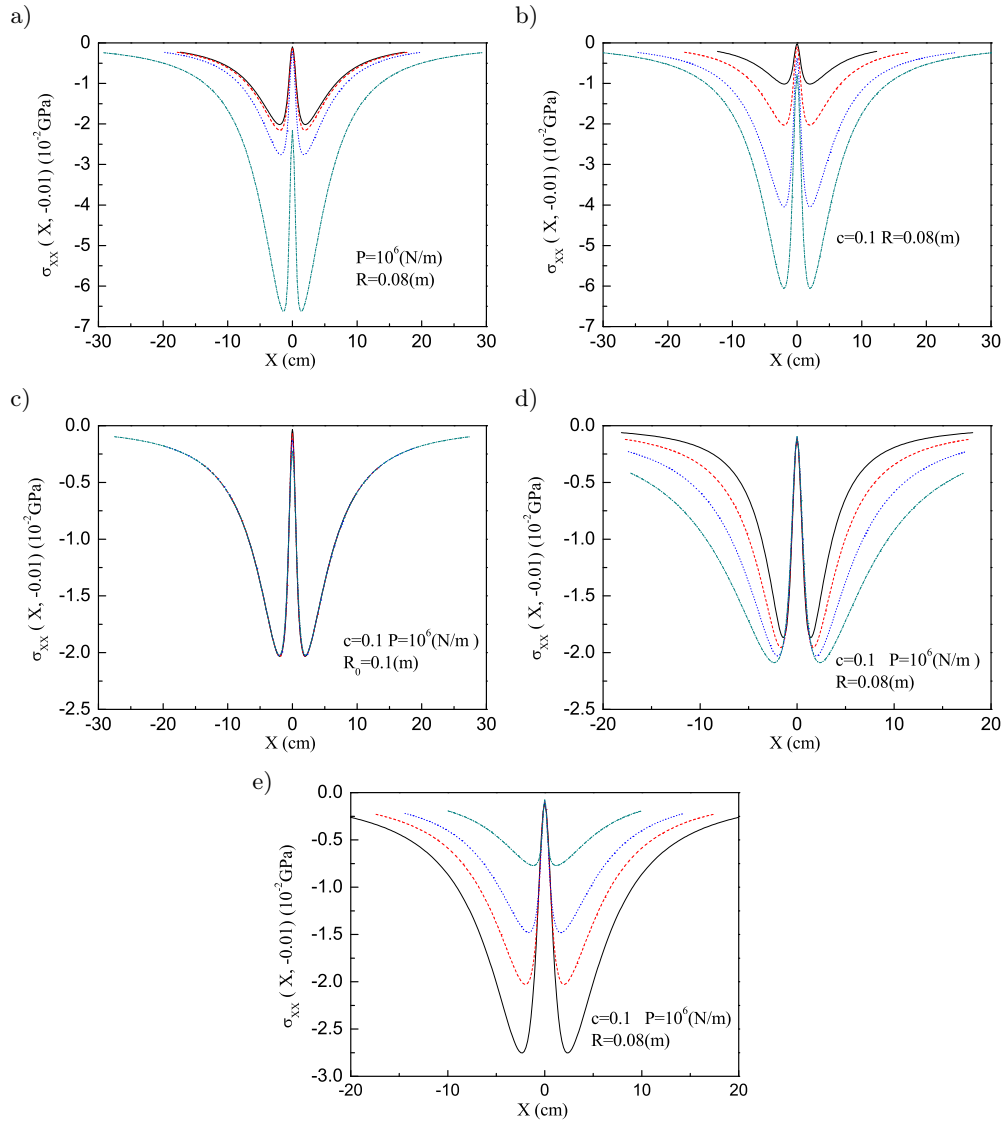


FIG. 10. The influence of a) velocity c , --- $c = 0.3$, \cdots $c = 0.6$, -.-.- $c = 0.9$, b) indentation force P , — $P = 0.5 \times 10^6$ N/m, --- $P = 1 \times 10^6$ N/m, \cdots $P = 3 \times 10^6$ N/m, -.-.- $P = 3 \times 10^6$ N/m, c) radius R , — $R = 0.25 \times R_0$, --- $R = 0.5 \times R_0$, \cdots $R = 1 \times R_0$, -.-.- $R = 2 \times R_0$, d) ratio E_{xx}/E_{xx0} , — $E_{xx}/E_{xx0} = 0.25$, --- $E_{xx}/E_{xx0} = 0.5$, \cdots $E_{xx}/E_{xx0} = 1$, -.-.- $E_{xx}/E_{xx0} = 2$, e) ratio E_{yy}/E_{yy0} , — $E_{yy}/E_{yy0} = 0.5$, --- $E_{yy}/E_{yy0} = 1$, \cdots $E_{yy}/E_{yy0} = 2$, -.-.- $E_{yy}/E_{yy0} = 8$, on the in-plane stress $\sigma_{XX}(X, 0)$ below the surface under a moving cylindrical punch.

the Young's modulus ratio E_{xx}/E_{xx0} , and e) decreasing the Young's modulus ratio E_{yy}/E_{yy0} . It deserves noting that Fig. 8 can be plotted either from Eq. (5.6) in view of Eq. (4.6) or from the second expression of Eq. (5.8), which justifies the correctness of the derivation for the case of the cylindrical punch.

Figure 9 indicates the influence of velocity c , indentation force P , radius R , ratio E_{xx}/E_{xx0} , and ratio E_{yy}/E_{yy0} on the surface in-plane stress $\sigma_{XX}(X, 0)$ under the moving cylindrical punch. As with the surface normal stress $\sigma_{YY}(X, 0)$, the surface in-plane stress $\sigma_{XX}(X, 0)$ is also zero at the edges of the cylindrical punch and its peak magnitude appears at the punch center. The methods that can be used to relieve the peak magnitude of the surface in-plane stress $\sigma_{XX}(X, 0)$ include: a) decreasing the moving velocity, b) decreasing the indentation force P , c) increasing the radius R , d) decreasing the Young's modulus ratio E_{xx}/E_{xx0} , and e) increasing the Young's modulus ratio E_{yy}/E_{yy0} , which are somewhat different from those used to relieve the peak magnitude of the surface normal stress $\sigma_{YY}(X, 0)$.

The influence of velocity c , indentation force P , radius R , ratio E_{xx}/E_{xx0} , and ratio E_{yy}/E_{yy0} on the in-plane stress $\sigma_{XX}(X, Y)$ below the surface under the moving cylindrical punch is depicted in Fig. 10. The magnitude of the in-plane stress $\sigma_{XX}(X, Y)$ increases from a local minimum at the punch center to a maximum, and then decays to a limiting value. The maximum of the magnitude of the in-plane stress $\sigma_{XX}(X, Y)$ increases with increasing velocity c , indentation force P or ratio E_{xx}/E_{xx0} , while decreases with increasing ratio E_{yy}/E_{yy0} . It seems that radius R has no significant influence on the in-plane stress $\sigma_{XX}(X, Y)$ below the surface under the moving cylindrical punch.

7. Conclusions

Contact analysis is performed for orthotropic materials under a frictionless moving punch possessing a flat or cylindrical profile. Fundamental solutions that can lead to real expressions of the physical quantities are derived for the orthotropic governing equation for each eigenvalue case. In order to solve the mixed boundary-value problem, unknown contact stress beneath the punch is introduced. Then, applying Galilean transformation and Fourier's transform technique, the closed-form solutions of the stated problem are expressed in terms of the elementary functions. Numerical results are given to graphically show the variations of contact behavior. Some main observations are drawn as follows:

- (i) there is high surface normal stress concentration in the vicinity of the flat punch edges, and the moving velocity and material properties have no effects on the surface normal stress under the flat punch;

- (ii) the surface in-plane stress is discontinuous around the edges of the flat punch, and the moving velocity and material properties greatly affect the distribution of the surface in-plane stress;
- (iii) the width of the contact region between the cylindrical punch and orthotropic materials can be adjusted through selecting the values of the moving velocity, indentation force, radius R , and material properties;
- (iv) the surface normal stress and the surface in-plane stress under the cylindrical punch are zero at the edges of the cylindrical punch, and their peak magnitude appears at the punch center, which can be relieved by choosing the values of the moving velocity, indentation force, radius R , and material properties.

These conclusions may be useful for material designing and optimization.

The dynamic contact for orthotropic materials concerned in this article is frictionless. The exact solution of frictionally dynamic contact for orthotropic materials will be presented in terms of elementary functions in the forthcoming work.

Acknowledgments

The authors would like to thank the anonymous reviewers for their helpful suggestions to this paper. This work was supported by the National Natural Science Foundation of China (51061015, 61063020, and 11261045).

Appendix A

1. Expressions of $\Theta_{mn}(\omega, Y)$ ($m = 1, 2, 3, n = 1, 2$) appearing in Eq. (3.13).

Case (i)

$$(A.1) \quad \Theta_{mn}(\omega, Y) = \Gamma_{mn} e^{o_n \omega Y},$$

where Γ_{mn} ($m = 1, 2, 3, n = 1, 2$) are given as

$$(A.2) \quad \Gamma_{1n} = D_{11} + D_{12} o_n l(o_n),$$

$$(A.3) \quad \Gamma_{2n} = D_{12} + D_{22} o_n l(o_n),$$

$$(A.4) \quad \Gamma_{3n} = D_{33} [o_n - l(o_n)].$$

Case (ii)

$$(A.5) \quad \begin{aligned} \Theta_{m1}(\omega, Y) &= [\Upsilon_{m1} \cos(\beta\omega Y) - \Upsilon_{m2} \sin(\beta\omega Y)] e^{\alpha\omega Y}, \\ \Theta_{m2}(\omega, Y) &= [\Upsilon_{m2} \cos(\beta\omega Y) + \Upsilon_{m1} \sin(\beta\omega Y)] e^{\alpha\omega Y} \end{aligned}$$

where Υ_{mn} ($m = 1, 2, 3$, $n = 1, 2$) are given as

$$(A.6) \quad \begin{aligned} \Upsilon_{11} &= D_{11} + D_{12} \{ \alpha \operatorname{Re} [l(o_1)] - \beta \operatorname{Im} [l(o_1)] \}, \\ \Upsilon_{12} &= D_{12} \{ \alpha \operatorname{Im} [l(o_1)] + \beta \operatorname{Re} [l(o_1)] \}, \end{aligned}$$

$$(A.7) \quad \begin{aligned} \Upsilon_{21} &= D_{12} + D_{22} \{ \alpha \operatorname{Re} [l(o_1)] - \beta \operatorname{Im} [l(o_1)] \}, \\ \Upsilon_{22} &= D_{22} \{ \alpha \operatorname{Im} [l(o_1)] + \beta \operatorname{Re} [l(o_1)] \}, \end{aligned}$$

$$(A.8) \quad \begin{aligned} \Upsilon_{31} &= D_{33} \{ \alpha - \operatorname{Re} [l(o_1)] \}, \\ \Upsilon_{32} &= D_{33} \{ \beta - \operatorname{Im} [l(o_1)] \}. \end{aligned}$$

2. Expressions of $T_{mn}(X, Y)$ ($m = 1, 2, 3$, $n = 1, 2$) appearing in Eq. (5.3).

Case (i)

$$(A.9) \quad T_{mn}(X, Y) = \Gamma_{mn} \Phi_{mn}(X, Y),$$

where

$$(A.10) \quad \Phi_{1n}(X, Y) = \Phi_{2n}(X, Y) = \frac{\sqrt{\phi_{2n}^2 - X^2}}{\phi_{2n}^2 - \phi_{1n}^2},$$

$$\Phi_{3n}(X, Y) = \operatorname{sgn}(X) \frac{\sqrt{X^2 - \phi_{1n}^2}}{\phi_{2n}^2 - \phi_{1n}^2},$$

$$(A.11) \quad \begin{aligned} \phi_{1n} &= \frac{1}{2} \left(\sqrt{(X+C)^2 + (o_n Y)^2} - \sqrt{(X-C)^2 + (o_n Y)^2} \right), \\ \phi_{2n} &= \frac{1}{2} \left(\sqrt{(X+C)^2 + (o_n Y)^2} + \sqrt{(X-C)^2 + (o_n Y)^2} \right), \end{aligned}$$

where $\operatorname{sgn}(\cdot)$ stands for the sign function.

Case (ii)

$$(A.12) \quad \begin{aligned} T_{m1}(X, Y) &= \frac{1}{2} [\Upsilon_{m1} H_{m1}(X, Y) - \Upsilon_{m2} H_{m2}(X, Y)], \\ T_{m2}(\omega, Y) &= \frac{1}{2} [\Upsilon_{m2} H_{m1}(X, Y) + \Upsilon_{m1} H_{m2}(X, Y)], \end{aligned}$$

where

$$(A.13) \quad \begin{aligned} H_{1n}(X, Y) &= H_{2n}(X, Y) = II_{n1}(X, Y) + II_{n2}(X, Y), \quad n = 1, 2, \\ H_{31}(X, Y) &= II_{21}(X, Y) - II_{22}(X, Y), \\ H_{32}(X, Y) &= -II_{11}(X, Y) + II_{12}(X, Y), \end{aligned}$$

$$(A.14) \quad \begin{aligned} \Pi_{1n}(X, Y) &= \frac{\sqrt{\theta_{n2}^2 - X_n^2}}{\theta_{n2}^2 - \theta_{n1}^2}, \quad n = 1, 2, \\ \Pi_{2n}(X, Y) &= \operatorname{sgn}(X_n) \frac{\sqrt{X_n^2 - \theta_{n1}^2}}{\theta_{n2}^2 - \theta_{n1}^2}, \quad n = 1, 2, \end{aligned}$$

with

$$(A.15) \quad \theta_{11} = \frac{1}{2} \left(\sqrt{(X_1 + C)^2 + (\alpha Y)^2} - \sqrt{(X_1 - C)^2 + (\alpha Y)^2} \right),$$

$$(A.16) \quad \theta_{12} = \frac{1}{2} \left(\sqrt{(X_1 + C)^2 + (\alpha Y)^2} + \sqrt{(X_1 - C)^2 + (\alpha Y)^2} \right),$$

$$(A.17) \quad \theta_{21} = \frac{1}{2} \left(\sqrt{(X_2 + C)^2 + (\alpha Y)^2} - \sqrt{(X_2 - C)^2 + (\alpha Y)^2} \right),$$

$$(A.18) \quad \theta_{22} = \frac{1}{2} \left(\sqrt{(X_2 + C)^2 + (\alpha Y)^2} + \sqrt{(X_2 - C)^2 + (\alpha Y)^2} \right),$$

$$(A.19) \quad X_1 = \beta Y + X, \quad X_2 = \beta Y - X.$$

3. Expressions of $I_{mn}(X, Y)$ ($m = 1, 2, 3$, $n = 1, 2$) appearing in Eq. (5.8)

Case (i)

$$(A.20) \quad I_{mn}(X, Y) = \Gamma_{mn} \Psi_{mn}(X, Y),$$

where

$$(A.21) \quad \begin{aligned} \Psi_{1n}(X, Y) &= \Psi_{2n}(X, Y) = \frac{\sqrt{\phi_{2n}^2 - X^2} + o_n Y}{C}, \\ \Psi_{3n}(X, Y) &= \frac{X - \operatorname{sgn}(X) \sqrt{X^2 - \phi_{1n}^2}}{C}, \end{aligned}$$

where ϕ_{pn} ($p, n = 1, 2$) are given in Eq. (A.11).

Case (ii)

$$(A.22) \quad \begin{aligned} I_{m1}(X, Y) &= \frac{1}{2} [\Upsilon_{m1} \Delta_{m1}(X, Y) - \Upsilon_{m2} \Delta_{m2}(X, Y)], \\ I_{m2}(\omega, Y) &= \frac{1}{2} [\Upsilon_{m2} \Delta_{m1}(X, Y) + \Upsilon_{m1} \Delta_{m2}(X, Y)], \end{aligned}$$

where

$$(A.23) \quad \begin{aligned} \Delta_{1n}(X, Y) &= \Delta_{2n}(X, Y) = K_{n1}(X, Y) + K_{n2}(X, Y), \quad n = 1, 2, \\ \Delta_{31}(X, Y) &= K_{21}(X, Y) - K_{22}(X, Y), \\ \Delta_{32}(X, Y) &= -K_{11}(X, Y) + K_{12}(X, Y), \end{aligned}$$

$$(A.24) \quad \begin{aligned} K_{1n}(X, Y) &= \frac{\sqrt{\theta_{n2}^2 - X_n^2} + \alpha Y}{C}, \quad n = 1, 2, \\ K_{2n}(X, Y) &= \frac{X_n - \operatorname{sgn}(X_n)\sqrt{X_n^2 - \theta_{n1}^2}}{C}, \quad n = 1, 2, \end{aligned}$$

where θ_{kl} ($k, l = 1, 2$) and X_k ($k = 1, 2$) are given, respectively, in Eqs. (A.15)–(A.19).

References

1. H. HERTZ, *On the contact of elastic solids*, Journal Für Die Reine Und Angewandte Mathematik, **92**, 156–171, 1882.
2. G.M.L. GLADWELL, *Contact Problems in the Classical Theory of Elasticity*, Sijthoff and Noordhof, The Netherlands, 1980.
3. K.L. JOHNSON, *Contact Mechanics*, Cambridge University Press, Cambridge, 1985.
4. D.A. HILLS, D. NOWELL, A. SACKFIELD, *Mechanics of Elastic Contacts*, Butterworth-Heinemann, Oxford, 1993.
5. J.W. NAM, J. HAWONG, S.J. HAN, S.H. PARK, *Contact stress of O-ring under uniform squeeze rate by photoelastic experimental hybrid method*, Journal of Mechanical Science and Technology, **22**, 2337–2349, 2008.
6. T.F. CONRY, A. SEIREG, *A mathematical programming method for design of elastic bodies in contact*, ASME Journal of Applied Mechanics, **93**, 387–392, 1971.
7. K.P. SINGH, B. PAUL, *Numerical solution of non-Hertzian elastic contact*, ASME Journal of Applied Mechanics, **41**, 484–490, 1974.
8. B. PAUL, J. HASHEMI, *Contact pressures on closely conforming elastic bodies*, ASME Journal of Applied Mechanics, **48**, 543–548, 1981.
9. K.J. BATHE, *Finite Element Procedures in Engineering Analysis*, Prentice-Hall, Englewood Cliffs, 1982.
10. T.J. HUGHES, *The Finite Element Method-Linear Static and Dynamic Finite Element Analysis*, Prentice-Hall, Englewood Cliffs, 1987.
11. M. PIMSARN, K. KAZEROUNIAN, *Pseudo-interference stiffness estimation, a highly efficient numerical method for force evaluation in contact problems*, Engineering with Computers, **19**, 85–91, 2003.
12. S. KRENK, *On the elastic constants of plane orthotropic elasticity*, Journal of Composite Materials, **13**, 108–116, 1979.
13. N.J. PAGANO, *Exact solutions for rectangular bidirectional composites and sandwich plates*, Journal of Composite Materials, **4**, 20–34, 1970.
14. T.M. TAN, C.T. SUN, *Use of statical indentation laws in the impact analysis of laminated composite plates*, ASME Journal of Applied Mechanics, **5**, 6–12, 1985.
15. E. WU, C.S. YEN, *The contact behavior between laminated composite plates and rigid spheres*, ASME Journal of Applied Mechanics, **61**, 60–66, 1994.

16. V.A. SVEKLO, *Boussinsq type problems for the anisotropic half-space*, ASME Journal of Applied Mechanics, **28**, 1099–1105, 1964.
17. V.A. SVEKLO, *The action of a stamp on an elastic anisotropic half-space*, Journal of Applied Mathematics and Mechanics, **34**, 165–171, 1970.
18. V.A. SVEKLO, *Hertz problems on compression of anisotropic bodies*, Journal of Applied Mathematics and Mechanics, **38**, 1023–1027, 1974.
19. A.A. SHI, Y. LIN, T.C. OVAERT, *Indentation of an orthotropic half-space by a rigid ellipsoidal indenter*, Journal of Tribology, **125**, 223–231, 2003.
20. J.R. WILLIS, *Hertzian contact of anisotropic bodies*, Journal of the Mechanics and Physics of Solids, **14**, 163–176, 1966.
21. S.R. SWANSON, *Hertzian contact of orthotropic plates*, International Journal of Solids and Structures, **41**, 1945–1959, 2004.
22. J. DE, B. PATRA, *Dynamic punch problems in an orthotropic elastic half-space*, Indian Journal of Pure and Applied Mathematics, **25**, 767–776, 1994.
23. T. IAMANIDZE, M. LOSABERIDZE, *On dynamic effect caused by moving punches on elastic half-plane with the account of friction force*, Bulletin of the Georgian National Academy of Sciences, **4**, 39–43, 2010.
24. E. LIRA-VERGARA, C. RUBIO-GONZALEZ, *Dynamic stress intensity factors around two parallel cracks in an infinite-orthotropic plane subjected to incident harmonic stress waves*, International Journal of Fracture, **135**, 285–309, 2005.

Received November 15, 2012; revised version January 30, 2013.
